Dissipative quantum dynamics: Driven molecular vibrations

Mingwhei Tung
Department of Physics, Swarthmore College, Swarthmore, Pennsylvania 19081

Jian-Min Yuan
Department of Physics and Atmospheric Science, Drexel University, Philadelphia, Pennsylvania 19104
(Received 16 March 1987)

We have studied quantum-mechanical behavior of a driven Morse oscillator coupled to a bath of harmonic oscillators. The purpose is to compare the quantum behavior of such a system with the classical solutions of a driven damped Morse oscillator. We start with the quantum Liouville equation, in which the Hamiltonian of the Morse oscillator is expressed in terms of generators of an su(2) Lie algebra. This algebra and the Markovian approximation allow us to derive the generalized master equation (for the reduced density matrix of the Morse oscillator), which contains level-dependent energy and phase relaxation terms. We have numerically integrated the differential equations of the matrix elements to obtain the time evolution of the reduced density matrix and the energy of the Morse oscillator. We show that the energy of the Morse oscillator in general varies with time and eventually reaches an asymptotic oscillatory state. The mean energy value of the asymptotic oscillatory state is studied as a function of the relaxation rates and laser frequency and amplitude. Vibrational distributions have also been found as functions of laser frequency and amplitude. The shape of the distribution changes gradually as laser amplitude increases; it first peaks at the ground state at a small field amplitude, then it peaks at some excited state at a large field amplitude, and for an amplitude in between it can have two maxima. This bimodal vibrational distribution reflects the bistability observed in the classical and semiclassical models. Thus bistability exists in quantum results, not as a hysteresis loop, but as a bimodal distribution. Finally, we show that as laser intensity increases, the time series of the oscillator energy evolves from regular to quasiperiodic behavior, and eventually a chaotic-looking series appears.

I. INTRODUCTION

It has been shown that classical solutions of the driven damped Morse oscillator

$$\ddot{x}+\gamma\dot{x}+e^{-x}(1-e^{-x})=A\cos(\omega t) \tag{1.1}$$

exhibit bistable behavior.[1,2] This means for a certain set of parameter values: A, ω, and γ, the $(x,\dot{x})$ phase space made of initial states leading to bound motion can be divided into basins of attraction for two attractors.[3] We shall call the attractor with a smaller amplitude ($x_{\max}$) the lower branch and that with a larger amplitude the upper branch. The attractors are of either periodic or chaotic type.[1,4] It can be shown that chaotic attractor can exist on both branches and the scenario leading to chaos is period-doubling bifurcations.

Such bistability exists[2,5] also in an approximate quantum-mechanical study of the dynamical behavior of an anharmonic oscillator which is in contact with a bath and is driven by a classical field.[6] The Hamiltonian of the oscillator, given by

$$H_a=a^{\dagger}a\hbar\omega-a^{\dagger}a(a^{\dagger}a+1)\hbar\varepsilon\ , \tag{1.2}$$

can be obtained from the expression of the Morse eigenvalues by substituting the number operator $a^{\dagger}a$ for the vibrational quantum number. The dynamics of this oscillator is described by the quantum Liouville equation in which the effects of bath are included as two relaxation terms; one each for the phase and energy relaxation. The equations of motion of the expectation values of operators $\langle a\rangle$, $\langle a^{\dagger}\rangle$, $\langle a^{\dagger}a\rangle$, ... can then be constructed. This infinite hierarchy of equations can be truncated by introducing factorization ansatz and a set of three first-order nonlinear differential equations for $\langle a\rangle$, $\langle a^{\dagger}\rangle$, $\langle a^{\dagger}a\rangle$ is then obtained.[6] Because the factorization techniques used are typical of most semiclassical models, we shall call this approach a semiclassical one below. The steady states of the above-mentioned set of equations are roots of a cubic equation and can be described by a cusp catastrophe,[5,2] when the steady-state values of $\langle a^{\dagger}a\rangle$ are plotted as a function of the driving field amplitude and frequency. We note that, the steady oscillations of Eq. (1.1) can also be described by a cusp catastrophe, when the amplitude of oscillation, $x_{\max}$, or the average oscillator energy is plotted against the same control parameters. However, there is a difference between results of these two models, the steady states of the semiclassical model on the upper and lower branches of the cusp catastrophe are always stable (if the ratio between the transverse and longitudinal relaxation time is taken to be less than 2, the physical upper bound), but the periodic states of the classical solutions on both the upper and lower branches can become unstable and chaos may arise as a result. On the other hand, since Eq. (1.2) is not exactly a Morse Hamiltonian, only a

Hamiltonian which yields Morse eigenvalues in the harmonic basis, we cannot draw conclusions about the comparison between the quantal versus classical behavior based on this model alone.

The objective of this paper is to present a more accurate quantum-mechanical study of the driven damped Morse oscillator problem. A legitimate way of introducing damping in a quantal approach is to start with a larger system in which the system of interest is in contact with a reservoir, which can be approximated by a large number of harmonic oscillators.[7] This was the procedure adopted in the semiclassical treatment.[5,6] Our system is a one-dimensional Morse oscillator whose Hamiltonian is expressed in terms of generators of an su(2) Lie algebra.[8,9] A generalized master equation for such an oscillator when coupled to a harmonic bath through linear coupling terms has been derived before.[10,11] We shall outline the procedure in the next section and generalize it to include some bilinear coupling terms. The time evolution equation of the density matrix and an application of it to a simple model will be presented. In Sec. III we derive the generalized master equation for a Morse oscillator pumped by a classical monochromatic field. Also derived are the generalized master equation and the temporal evolution equations of the matrix elements for the combined Morse oscillator plus reservoir plus field system. Results of numerical integration will be presented in Sec. IV, where we show how the energy and phase relaxation rates, the driving intensity and frequency affect the energy absorption efficiency of the oscillator. We show also how vibrational distributions vary with these factors and discuss why these results suggest the existence of bistable behavior. The time series of the oscillator energy reaches a steady oscillatory state, which varies from a seemingly periodic state to a quasiperiodic and eventually to a chaotic-looking state as field intensity increases. We shall analyze these results by using fast-Fourier-transform (FFT) spectra. Finally, in Sec. V we shall discuss the significance of our results.

II. THE FIELD-FREE SYSTEM: MORSE OSCILLATOR PLUS RESERVOIR

The Hamiltonian of a Morse oscillator plus reservoir system can be written as

$$H=H_S+H_R+H_{SR} , \tag{2.1}$$

where the Morse Hamiltonian H_S, the Hamiltonian of the reservoir H_R and the interaction between them, H_{SR}, are defined, respectively, by

$$H_S=\hbar\omega(A^+A^-+I_0/2) , \tag{2.2a}$$

$$H_R=\sum_{j=1}^{\infty}\hbar\omega_j a_j^\dagger a_j , \tag{2.2b}$$

$$H_{SR}=H_1+H_2 . \tag{2.2c}$$

In Eqs. (2.2), A^+, A^-, and I_0 are generators of an su(2) Lie algebra which satisfy the following commutation relations:

$$\begin{aligned}&[A^-,A^+]=I_0 ,\\ &[A^\pm,I_0]=\pm 2x_0A^\pm .\end{aligned} \tag{2.3}$$

A^+ and A^- function as the raising and lowering operators of the Morse eigenstates as given by the following relations:

$$A^+|m\rangle=[(1-x_0m)(m+1)]^{1/2}|m+1\rangle , \tag{2.4a}$$

$$A^-|m\rangle=\{[1-x_0(m-1)]m\}^{1/2}|m-1\rangle , \tag{2.4b}$$

$$I_0|m\rangle=(1-2x_0m)|m\rangle . \tag{2.4c}$$

In Eqs. (2.4), x_0 is an anharmonic parameter, related to one-half of the total number of bound states. Levine[8,9] has shown that the exact Morse eigenvalues and eigenfunctions are obtainable from H_S [Eq. (2.2a)]. $a_j^\dagger$ and a_j in Eqs. (2.2) are the ordinary creation and annihilation operators of a harmonic oscillator with frequency ω_j. The interaction Hamiltonian H_{SR} contains the linear and bilinear terms, which are given separately by

$$H_1=\sum_{j=1}^{\infty}\hbar(\kappa_jA^+a_j+\kappa_j^*a_j^\dagger A^-) , \tag{2.5}$$

$$H_2=\hbar\Gamma A^+A^- , \tag{2.6}$$

in which Γ is an operator in the reservoir space and κ_j is a complex constant.[12]

We can derive the generalized master equation for the Morse oscillator, starting with the Liouville equation

$$dW(t)/dt=-i[L_S+L_R+L_{SR}]W(t) , \tag{2.7}$$

where $W(t)$ is the statistical density operator for the entire system and L_iX is defined by

$$L_iX=[H_i,X]/\hbar . \tag{2.8}$$

The procedure that we shall follow is that of Ref. 11, but here we include not only linear interaction terms but also a bilinear one.[12] We assume weak interaction between the system and each degree of freedom of the reservoir and that the reservoir is never far from thermal equilibrium and any deviations from equilibrium are rapidly eliminated due to some dissipative mechanisms. Therefore $W(t)$ can be written as

$$W(t)=\rho(t)W_R^\beta , \tag{2.9}$$

where $\rho(t)$ is the reduced density operator for the system defined by

$$\rho(t)=\mathrm{Tr}_R[W(t)] \tag{2.10}$$

and W_R^β by

$$W_R^\beta=e^{-\beta H_R}/\mathrm{Tr}_R(e^{-\beta H_R}) . \tag{2.11}$$

Besides the weak-interaction approximation we introduce furthermore the Markovian approximation that the relaxation time of the bath correlation functions is much shorter than the characteristic time of the system, the generalized master equation can be written in the following form:[10,11]

$$d\rho/dt=-iL_S\rho+g^2\int_0^\infty \exp(-i\omega x_0\tau)\{\langle B(\tau)B^\dagger\rangle_0[\exp(i\omega I_0\tau)A^-\rho(t),A^+]+\langle B^\dagger B(\tau)\rangle_0[A^+,\rho(t)\exp(i\omega I_0\tau)A^-]$$
$$+\langle BB^\dagger(\tau)\rangle_0[A^-,\rho(t)\exp(-i\omega I_0\tau)A^+]$$
$$+\langle B^\dagger(\tau)B\rangle_0[\exp(-i\omega I_0\tau)A^\dagger\rho(t),A^-]\}d\tau$$
$$+\eta\{[A^+A^-\rho(t),A^+A^-]+[A^+A^-,\rho(t)A^+A^-]\}\ , \tag{2.12}$$

where

$$B=\sum_j \kappa_j a_j/g\ ,$$
$$B(t)=\exp(iH_R t/\hbar)B\exp(-iH_R t/\hbar)\ ,$$
$$g=(\sum_j |\kappa_j|^2)^{1/2}\ , \tag{2.13}$$
$$\eta=\pi\sum_{m,n}|\Gamma_{mn}|^2(W_R^\beta)_{mm}\delta((\omega_R)_{mn})\ .$$

$(\omega_R)_{mn}$ is the frequency difference of the bath in m and n states. In deriving Eq. (2.12) we have omitted the weak interference term between H_1 and H_2. One can easily show Eq. (2.12) reduces to the master equation of a harmonic oscillator coupled to a harmonic bath in the harmonic limit $x_0\to 0$.[13–15]

The time evolution equation of the off-diagonal elements of the density matrix ρ_{km} can be derived from Eq. (2.12) by sandwiching this equation between kth and mth Morse eigenstates and utilizing Eqs. (2.4). The procedure is similar to that used in Ref. 11. We obtain[10]

$$d\rho_{km}/dt=-i\omega_{km}\rho_{km}+[\overline{(k+1)(m+1)}]^{1/2}(\gamma_{\downarrow k+1}+\gamma_{\downarrow m+1})\rho_{k+1,m+1}$$
$$-[\bar{k}\gamma_{\downarrow k}+\bar{m}\gamma_{\downarrow m}+\overline{(k+1)}\gamma_{\uparrow k}+\overline{(m+1)}\gamma_{\uparrow m}+\eta(\bar{k}-\bar{m})^2]\rho_{km}+(\bar{k}\bar{m})^{1/2}[\gamma_{\uparrow(k-1)}+\gamma_{\uparrow(m-1)}]\rho_{k-1,m-1}\ , \tag{2.14}$$

where we have dropped the imaginary part of the coefficients, corresponding to small level shifts.[14] ω_{km} is the frequency difference between the kth and mth levels of the Morse oscillator and given by

$$\omega_{km}=\omega(k-m)[1-x_0(k+m)]\ . \tag{2.15}$$

Other symbols are defined as

$$\sigma_m=\pi|\kappa_j|^2D(\omega_j)|_{\omega_j=\Delta E(m)/\hbar}\ ,$$
$$n_m=[e^{\Delta E(m)/k_BT}-1]^{-1}\ ,$$
$$\gamma_{\downarrow m}=\sigma_m(n_m+1)\ , \tag{2.16}$$
$$\gamma_{\uparrow m}=\sigma_{m+1}n_{m+1}\ ,$$
$$\Delta E(m)=\hbar\omega[1-(2m-1)x_0]\ ,$$
$$\bar{m}=m[1-x_0(m-1)]\ .$$

The spectral density distribution of the bath $D(\omega_j)$ was introduced when we integrate over the bath frequency in evaluating the correlation function in Eq. (2.12). For the diagonal elements the evolution equation becomes

$$d\rho_{mm}/dt=2\gamma_{\downarrow m+1}\overline{(m+1)}\rho_{m+1,m+1}$$
$$-2[\gamma_{\downarrow m}\bar{m}+\gamma_{\uparrow m}\overline{(m+1)}]\rho_{mm}$$
$$+2\gamma_{\uparrow(m-1)}\bar{m}\rho_{m-1,m-1}\ . \tag{2.17}$$

In the harmonic limit $x_0\to 0$ Eqs. (2.14)–(2.17) reduce to those of a harmonic oscillator in contact with a harmonic bath, namely, the equations obtained by replacing $\bar{m}$ by m and dropping the level dependence of the relaxation rates in the above equations. Equations (2.14) and (2.17) make clear that the effects of a Morse oscillator are that the energy relaxation coefficients are level dependent and the factor multiplying the coefficients, m, is replaced in the anharmonic case by a smaller number $\bar{m}$.

Other things to be noticed are the following.

(1) Equation (2.17) satisfies the detailed balance relation.

(2) A level couples only to its nearest neighbors is the result of the form of the couplings assumed in Eqs. (2.5) and (2.6).

(3) The level-independent phase relaxation coefficient η appears only in the equation of the diagonal elements, not in that of the off-diagonal elements.

(4) Unlike its harmonic analog, Eq. (2.17) is highly nonlinear in m and thus much more difficult to solve analytically.[13]

Equation (2.17) has many features different from its harmonic counterpart and to illustrate some of these features we have studied relaxation properties of a diatomic molecule in contact with a bath which has a flat spectral profile, namely, a constant $D(\omega)$. The molecular parameters used are approximately those of an HF molecule: $\omega=4140\ \text{cm}^{-1}$ and $x_0=0.0211$. To reduce the number of parameters involved we further assume all κ_j, thus σ_m, are identical. We shall drop the subscript of σ and use the value $\sigma=0.1^*\omega/2\pi$ in our calculation. Equation (2.17) can be rewritten into the following form:

$$d\rho_m/dt=2\sigma n_m\bar{m}\rho_{m-1}+2\sigma(n_{m+1}+1)\overline{(m+1)}\rho_{m+1}$$
$$-2\sigma[n_{m+1}\overline{(m+1)}-(n_m+1)\bar{m}]\rho_m\ , \tag{2.18}$$

where we have denoted ρ_{mm} by ρ_m. The matrix on the right-hand side has the following properties.

(1) It is tridiagonal.

(2) The sum of all the elements in each column is zero.

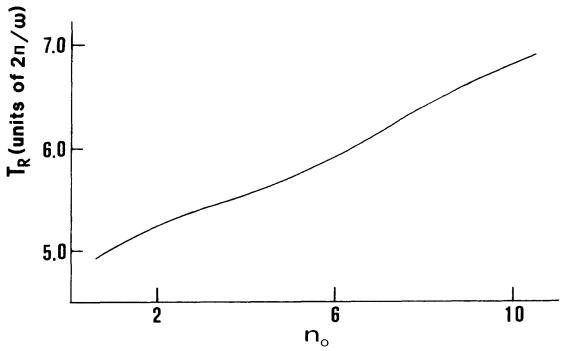

FIG. 1. Relaxation time (T_R) of the field-free Morse oscillator as a function of the initial vibrational quantum number n_0. T_R is scaled by $2\pi/\omega$. The damping coefficient is fixed at $\sigma=0.1^*\omega/(2\pi)$ and the temperature is at 300 K.

(3) All diagonal elements are negative and off-diagonal elements positive.

As proved in the Appendix, these properties guarantee that all eigenvalues of the matrix are real and nonpositive. Thus the dynamics should be simple. If the temperature is sufficiently low, all level populations decay exponentially except that of the ground state.

We integrate Eq. (2.18) by using the fourth-order Runge-Kutta method to obtain $\rho_m(t)$'s, and from them calculate the expectation value of the oscillator energy at time t according to the relation

$$\langle E(t)\rangle=\sum_m \rho_m(t)E_m \ , \tag{2.19}$$

where E_m is the mth Morse energy level. For the harmonic analog energy decays exponentially as given by the following formula:[13]

$$\langle E(t)\rangle=\langle E_0\rangle e^{-\lambda t}+n(\omega)(1-e^{-\lambda t})\hbar\omega \ , \tag{2.20}$$

where $\langle E_0\rangle$ is the initial energy and $n(\omega)$ the average excitation of each degree of freedom of the reservoir given by

$$n(\omega)=[e^{\hbar\omega/k_BT}-1]^{-1} \ , \tag{2.21}$$

and λ is the decay constant related to σ. In the case of the Morse oscillator the decay is almost exponential. We shall define the relaxation time as the time at which the energy decays to half of its initial value. Our results are presented in Fig. 1, where we have plotted the relaxation time (T_R) as a function of the initial excitation n_0. The results show that the relaxation time increases as n_0 increases, in consistency with the fact that the period increases with energy. In carrying out the calculation the temperature is taken to be 300 K, and we have checked numerically that the results are not sensitive to the temperature for the range of interest here.

III. THE FIELD-DRIVEN SYSTEMS

The Hamiltonian of a Morse oscillator driven by a classical field can be written as

$$H=H_S+H_{SF} \ , \tag{3.1}$$

where H_{SF} is given by the form

$$H_{SF}=\mu\varepsilon(A^++A^-)\cos(\omega_f t) \ . \tag{3.2}$$

We assume in H_{SF} that $\mu(A^++A^-)$ denotes the dipole moment operator and ε is the field amplitude. Since it is not known how to express the oscillator coordinate in terms of A^+, A^-, and I_0, we have used an expression for the dipole moment which yields the correct form in the harmonic limit. The master equation is given by

$$d\rho(t)/dt=-iL_S\rho-iL_{SF}\rho \ , \tag{3.3}$$

where L_{SF} is defined by Eq. (2.8), and the time-evolution equation for the matrix element becomes

$$\begin{aligned} d\rho_{km}/dt=&-i\omega_{km}\rho_{km}-i\Omega_R\cos(\omega_f t)\\ &\times\{\bar{k}^{1/2}\rho_{k-1,m}+\overline{(k+1)}^{1/2}\rho_{k+1,m}\\ &-\bar{m}^{1/2}\rho_{k,m-1}-\overline{(m+1)}^{1/2}\rho_{k,m+1}\} \ , \end{aligned} \tag{3.4}$$

where Ω_R is the Rabi rate defined by $\mu\varepsilon/\hbar$.

The total Hamiltonian for the driven dissipative system is

$$H=H_S+H_R+H_{SR}+H_{SF} \ . \tag{3.5}$$

The full master equation is obtained by adding the second term of the right-hand side of Eq. (3.3) to the Eq. (2.12). Similarly the full time evolution equation can be obtained by adding the new term in Eq. (3.4) to Eq. (2.14). In following this procedure we have neglected small interference terms that would arise from the coupling between H_{SF} and H_{SR}.

The ρ which satisfies the full time evolution equation oscillates rapidly with time due to the presence of $-i\omega_{km}\rho_{km}$ term. This fast oscillation can be removed by making the following transformation:

$$\rho_1 km=e^{i\omega_{km}t}\rho_{km} \ , \tag{3.6}$$

where ω_{km} is given by Eq. (2.15), to a rotating coordinate frame. The time evolution equation then becomes

$$\begin{aligned} d\rho_{1\,km}/dt=&(\bar{k}\bar{m})^{1/2}(\gamma_{\uparrow\,k-1}+\gamma_{\uparrow\,m-1})e^{-i[2(k-m)x_0]\omega t}\rho_{1\,k-1,m-1}\\ &+\overline{(k+1)}^{1/2}\overline{(m+1)}^{1/2}(\gamma_{\downarrow\,k+1}+\gamma_{\downarrow\,m+1})e^{i[2(k-m)x_0]\omega t}\rho_{1\,k+1,m+1}\\ &-[\bar{k}\gamma_{\downarrow k}+\bar{m}\gamma_{\downarrow m}+\overline{(k+1)}\gamma_{\uparrow k}+\overline{(m+1)}\gamma_{\uparrow m}+\eta(\bar{k}-\bar{m})^2]\rho_{1\,km}\\ &-\Omega_R\cos\omega_f t\{\bar{k}^{1/2}e^{-i[(2k-1)x_0-1]\omega t}\rho_{1\,k-1,m}+\overline{(k+1)}^{1/2}e^{i[(2k+1)x_0-1]\omega t}\rho_{1\,k+1,m}\\ &-\bar{m}^{1/2}e^{i[(2m-1)x_0-1]\omega t}\rho_{1\,k,m-1}-\overline{(m+1)}^{1/2}e^{-i[(2m+1)x_0-1]\omega t}\rho_{1\,k,m+1}\} \ . \end{aligned} \tag{3.7}$$

The transformed matrix ρ_1 is the one which has been evaluated numerically and results are presented in Sec. IV.

IV. RESULTS OF CALCULATIONS

We have solved Eq. (3.7) numerically by using the fourth-order Runge-Kutta method and present all results in this section. Because the computation time increase quadratically in $n_{\max}$, the total number of levels considered, we have calculated the density matrix as a function of time for only the lowest seven energy levels. As discussed below in some cases we have done calculations using a larger $n_{\max}$ (up to $n_{\max}=10$) to verify our findings are not caused by a smaller $n_{\max}$. In principle, the factors σ's, appearing in the energy relaxation rates γ's [see Eq. (2.16)] are level dependent, we shall assume, as in Eq. (2.18), that the special density of the bath is so flat that all the σ's can be considered equal. Of course this does not reduce our problem into a harmonic one, for $\overline{m}$ still is a function of the anharmonicity. Molecular parameters simulating the HF molecule, as given in Sec. II, will be used through out the calculations. All energy quantities are scaled by $\hbar\omega$ and time quantities scaled by $2\pi/\omega$. We summarize results below.

A. Effects of the relaxation rates on the time evolution of $\langle E(t)\rangle$

Since the system is driven by a sinusoidal external field, it will not reach any equilibrium state but some steady oscillatory state. The effect of increasing σ with all other parameters fixed is to shorten the transient and to lower the average energy of the Morse oscillator in the asymptotic oscillatory state. This also means that to pump energy efficiently into the molecule we need to increase the intensity. For most of the calculation below σ will be fixed at 0.05. This corresponds to a very small and unrealistic relaxation time, roughly 0.2 psec for HF. This value is chosen to speed up the calculation, otherwise the calculation will be forbiddingly long. The corresponding field strength used will therefore be unrealistically high. For example, $\alpha=(2\pi/\omega)\Omega_R=0.07$ corresponds to 1 TW/cm^2 for HF.

The effects of increasing the phase relaxation rate (η) is more interesting as illustrated in Fig. 2, where the parameters are set at $\omega_f=4000$ cm^{-1} and $\alpha=0.22$. For a $\eta=0.05$ or 0.15 we see the vibrational energy of the molecule oscillates with large amplitude as a function of time and eventually settles down to a steady oscillation with smaller amplitude. As η increases the large amplitude oscillation is damped out and $\langle E\rangle$ approaches the steady oscillation smoothly. The asymptotic energy averaged over several oscillating periods (which is usually order of magnitude longer than the optical period), $E_{\rm av}$ (not to be confused with $\langle E(t)\rangle$), first increases with η, then decreases as η increases beyond 0.45 as shown in Fig. 3. To understand the phenomenon we notice that η can be interpreted as level width. Because of the anharmonicity the Morse oscillator is hard to excite, but as level width increases the resonance condition becomes easier to satisfy, thus $E_{\rm av}$ increases. But when η increases above a certain value (0.45), the oscillator strength is spread out so thin within the level width that it hinders pumping. Incidently we point out that some of the effects of the rotational levels can also be included in the phase relaxation.[6] For the rest of the calculations reported in this section η is set at 0.2.

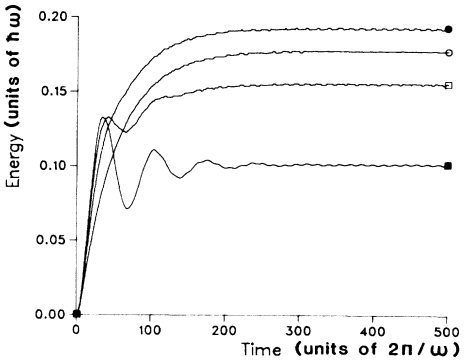

FIG. 2. Energy absorption of the Morse oscillator as a function of the phase relaxation rate η. The energy is scaled by $\hbar\omega$ and time by $2\pi/\omega$. The parameters ω_f, σ, and α are set at 4000 cm^{-1}, 0.05, and 0.22. The labeling symbols are the following: ■, $\eta=0.05$; □, $\eta=0.15$; ●, $\eta=0.35$; and ○, $\eta=0.80$.

B. Effects of varying the field intensity and frequency

With ω_f fixed at 3960 cm^{-1} we have plotted $E_{\rm av}$ as a function of the field amplitude, parametrized by α, in Fig. 4. We see that $E_{\rm av}$ increases with α as it should be, but what is worth noticing here is that there is a threshold value of α above which $E_{\rm av}$ rises suddenly and seems

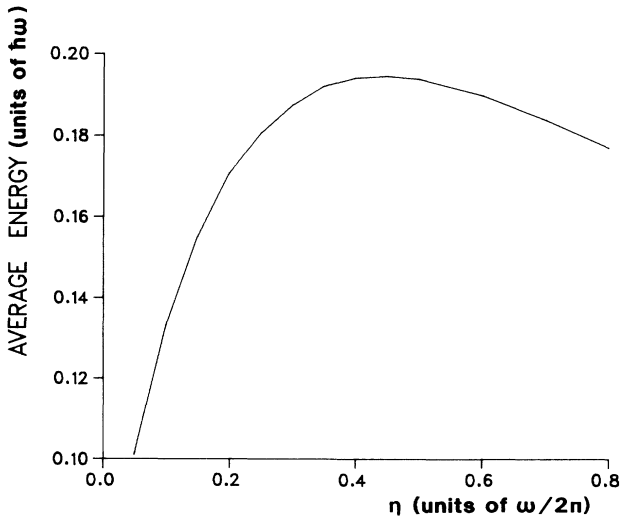

FIG. 3. The average asymptotic energy $E_{\rm av}$ of Fig. 2 plotted as a function of η.

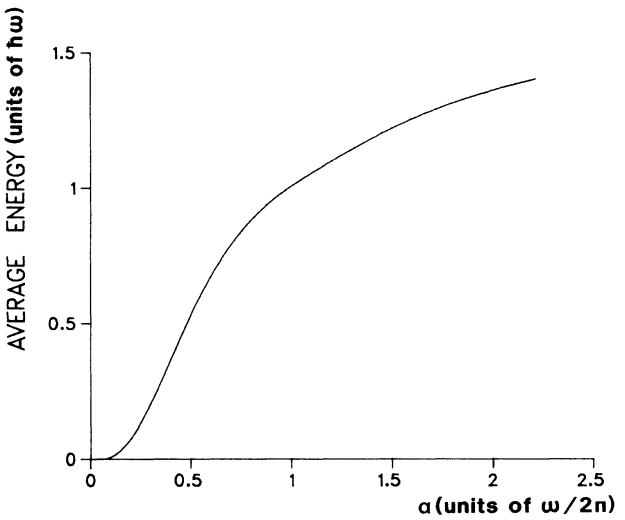

FIG. 4. The average asymptotic energy as a function of the scaled Rabi rate α, where ω_f, σ, and η are set at 3960 cm^{-1}, 0.05, 0.2. A similar curve has been obtained for $\omega_f = 3650$ cm^{-1}.

to rise only gradually at high fields. Such sudden rise can be expected from the bistable behavior observed in the classical and semiclassical studies of a Morse oscillator.[2,5] But the quantum results are different from the classical and semiclassical ones, mentioned in the Introduction, in the sense that no hysteresis has been found here. In fact that Eq. (3.7) is linear in ρ excludes the possibility of hysteresis. However, bistability does show up in quantum solutions, only in a different fashion. One hint to its existence is the sudden jump observed in Fig. 4. But more directly we can look at the asymptotic level population distribution, P_n, and see how it varies with α. For this purpose we have carried out a 10-level calculation to make sure that the highest level considered is not significantly populated and average P_n over about 50 optical periods. In Fig. 5 we have plotted P_n as a function of the quantum number n for several α's. For a small α the maximum of the distribution occurs at $n=0$. This maximum flattens out as α increases and a second maximum appears at a finite n ($n=3$). Eventually the peak at $n=0$ disappears and only the second maximum remains. Comparing Figs. 4 and 5 we can suggest that the lower branch (characterized in Fig. 4 by the flat part at small α) corresponds to a population distribution which peaks at the ground state, and the upper branch (the part at large α) corresponds to a distribution peaking at a finite n ($n=3$). For an intermediate α value we have a bimodal distribution, where both branches coexist, as shown more clearly in the insert of Fig. 5. Thus these quantum results provide us with a clear physical picture of the meaning of bistability observed in classical and semiclassical models. That is, bistability corresponds to two different kinds of population distributions, which can coexist. Which of these two distributions that the system is converging to (in the classical or semiclassical study) depends on the initial conditions. However, due to the statistical nature

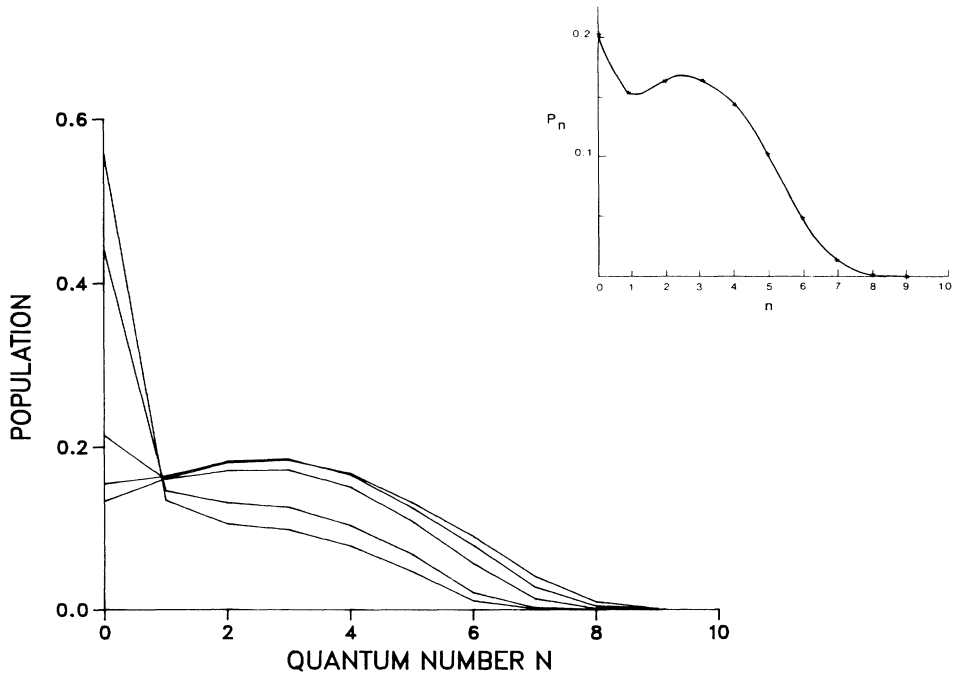

FIG. 5. The average asymptotic vibrational distribution as a function of the vibrational quantum number N for several driving amplitudes. The parameter values are the same as those given in Fig. 4. From the top curve down on the left (or from the bottom curve up on the right) α is given by 1.9, 2.2, 3.1, 3.8, and 4.4. The inset on the right corner is a continuous plot of the curve with $\alpha=3.1$.

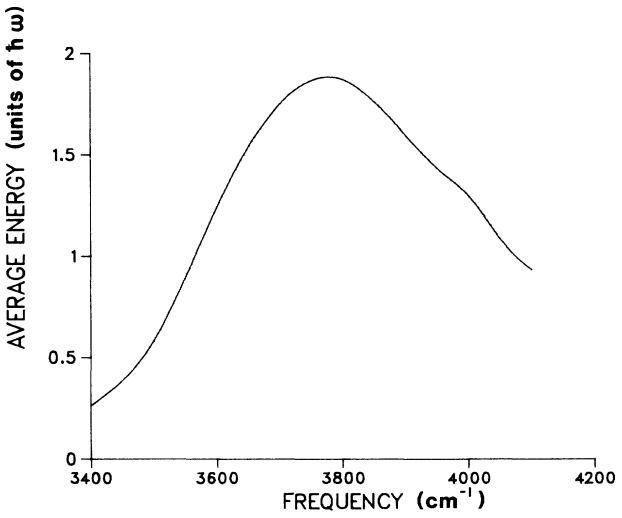

FIG. 6. The average asymptotic energy as a function of the driving frequency. The parameters α, σ, and η are set at 2.2, 0.05, and 0.2.

of quantum mechanics these two distributions are not mutually exclusive, instead an average behavior (bimodal distribution) appears. As discussed in Sec. V, bimodal vibrational distributions have already been observed in SF_6 experimentally.[16–18] It remains to verify whether the present mechanism is also responsible for their origin.

Effects of varying field frequency can be seen in Fig. 6, in which we have plotted $E_{\rm av}$ as a function of ω_f with α fixed at 2.2. $E_{\rm av}$ peaks at around $\omega_f = 3775$ cm^{-1}, which is significantly red shifted from the resonance frequency 4053 cm^{-1}. The shape of the curve is clearly asymmetric, which is again in consistency with the classical and semiclassical results that the steady behavior can be described by a cusp catastrophe.[2,5] The latter relation predicts a λ-shape curve with hysteresis when $E_{\rm av}$ is plotted against ω_f.[1,2,5] In a quantum system again only an average behavior is expected and the general signature which remains is the asymmetry of the curve.

C. Quantum dynamical instabilities

Classical solutions of a driven damped Morse oscillator show dynamical instability in the form of a cascade of period-doubling bifurcations leading to chaos. This is no evidence of such instability in the quantum solution, but an instability of a different kind seems to exist as revealed by a series of calculations presented in this section.

The time series of the Morse oscillator energy, $\langle E(t)\rangle$, in the stroboscopic representation for $\omega_f = 4040$ cm^{-1} and $\alpha = 0.022$ is shown in Fig. 7(a). It looks like a periodic orbit with a frequency less than 20 optical periods. Since the energy is recorded every optical period, this periodic orbit lives on a torus. The fast

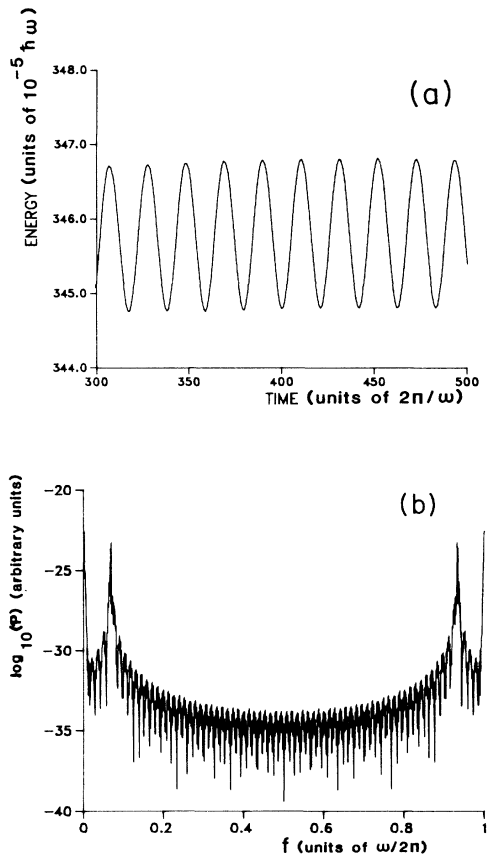

FIG. 7. (a) The time series of the oscillator energy $\langle E(t)\rangle$. The parameters ω_f, α, σ, and η are set at 4040 cm^{-1}, 0.022, 0.05, and 0.2. (b) The FFT power spectrum, $\log_{10}[P(f)]$, computed from the time series of (a).

Fourier transform spectrum of this time series, as shown in Fig. 7(b), indeed shows a dominant frequency at 14.6. In Fig. 8(a) a similar time series for $\omega_f = 4000$ cm^{-1} and $\alpha = 0.07$ is shown. It is clear that there are at least two dominant frequencies; a fast oscillation with a period of about 15 optical periods and its amplitude is modulated by a slow oscillation with a period of about 70. It is not clear whether the series is quasiperiodic or actually periodic. Its FFT spectrum in Fig. 8(b) shows several frequencies. In the order of decreasing intensity the periods are $T_1 = 14.7$ (with a shoulder at $T_1' = 13.4$), $T_2 = 71.4$, $T_3 = 33.3$, and $T_4 = 23.1$ in units of optical periods. T_1 is by far the dominating period. At the same ω_f when α is increased to 0.22, the time series in Fig. 9(a) shows again a fast oscillation on top of a slow modulation, which is more pronounced than Fig. 8(a). Its FFT in Fig. 9(b) shows the same characteristic periods: $T_1 = 14.6$, $T_2 = 71.7$, $T_3 = 32.7$, $T_1' = 13.4$, and $T_4 = 23.2$ in the order of decreasing intensity. T_1 still dominates, but T_2 is also quite pronounced and T_1', on the other hand, weakens.

For $\alpha = 0.81$ the time series becomes more complicated and the FFT spectrum shows several competing frequencies with noise background as shown in Figs. 10(a)

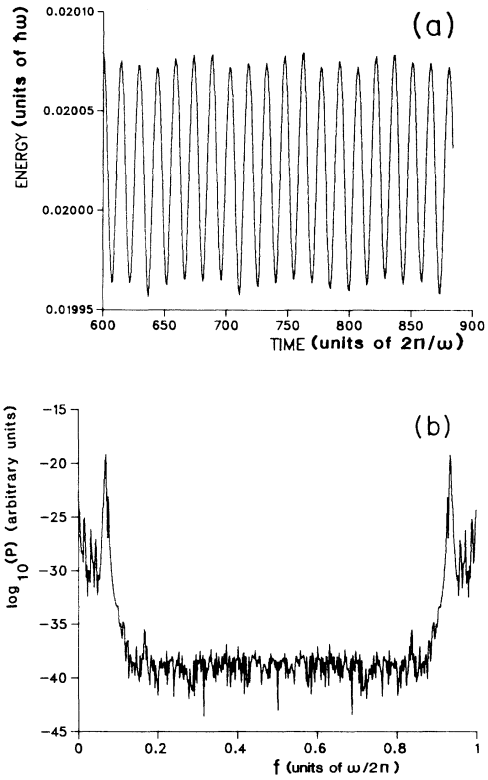

FIG. 8. (a) The time series of the oscillator energy $\langle E(t)\rangle$. The parameters ω_f, α, σ, and η are set at 4000 cm^{-1}, 0.07, 0.05, and 0.2. (b) The FFT power spectrum, $\log_{10}[P(f)]$, computed from the time series of (a).

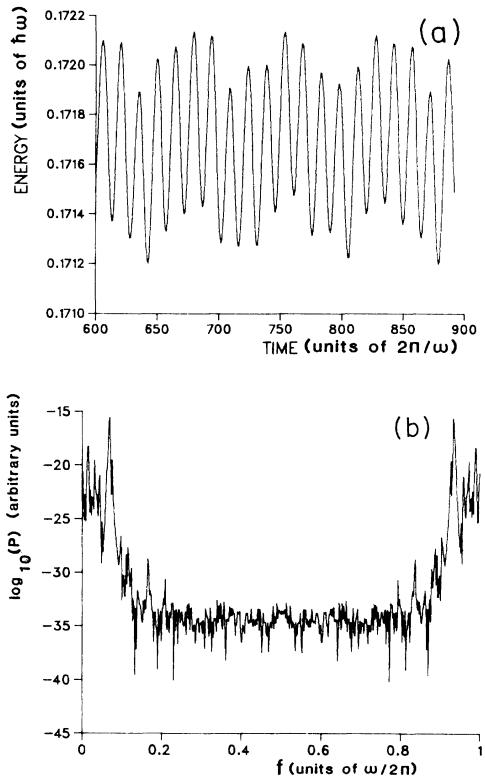

FIG. 9. (a) The time series of the oscillator energy $\langle E(t)\rangle$. The parameters ω_f, α, σ, and η are set at 4000 cm^{-1}, 0.22, 0.05, and 0.2. (b) The FFT power spectrum, $\log_{10}[P(f)]$, computed from the time series of (a).

and 10(b). In the order of decreasing intensity the dominating periods are $T_1=14.6$, $T_2=74.2$, $T_3=30.1$, $T_5=8.66$, and $T_4=23.4$. When α increased to 1.57, the time series shown in Fig. 11(a) becomes much more irregular. Its FFT spectrum in Fig. 11(b) is qualitatively different from results of weaker fields. Here the periods of decreasing intensity are $T_3=33.44$, $T_1=14.6$, $T_5=8.75$, $T_6=41.8$, $T_2=71.7$, and $T_7=6.4$. T_3 has become now the most pronounced period, and T_1 and T_2 still plays a role but becomes weakened. The characteristic periods T_1' and T_4 disappear, and T_6 and T_7 appear. Here the broad-noised background signifies the chaotic-looking behavior. But we have included Figs. 11 here for the reference purpose only, for the time series in Fig. 11(a) and even longer trials have not reached steady oscillatory state yet.

Unfortunately due to the great amount of computer time involved in the calculation we have not unraveled the underlying bifurcation mechanism of the series, but it is clearly not the period-doubling bifurcation scenario, as seen in the classical or semiclassical models.[1,19] One attempt we did make is to calculate the maximal Lyapunov exponent from the above time series.[20] In general the Lyapunov exponent is very small, of the order of 10^{-5}, with an uncertain sign. If the results are trustable, it may simply imply that all the above time series belong to quasiperiodic behavior or small deviation from it.

We also notice the characteristic frequencies, at least, the dominant ones are mainly determined by the driving frequency and not much affected by the intensity. For example, the dominant periods for $\omega_f=3920$, 3960, 4000, and 4040 cm^{-1} are, respectively, around 9, 11, 15, and 20 optical periods.

V. DISCUSSIONS

Vibrational bistability shows up as a hysteresis loop in the classical and semiclassical calculations of the molecular response, when field frequency or strength is varied adiabatically. But as long as the generalized master equation is linear in the reduced density matrix hysteresis does not exist in a quantum approach. Instead, bistability manifests itself in the present approach as a bimodal vibrational distribution. This is somewhat similar to the situation in optical bistability, where solution of the Fokker-Planck equation shows up also as bimodal distribution.[21,22] The difference is that the population here is a function of a discrete variable, the vibrational quantum number, not a continuous one. The bimodal distribution implies that two characteristic vibrational distributions exist; that is, a fraction of molecules is found to be highly excited and another fraction barely excited.

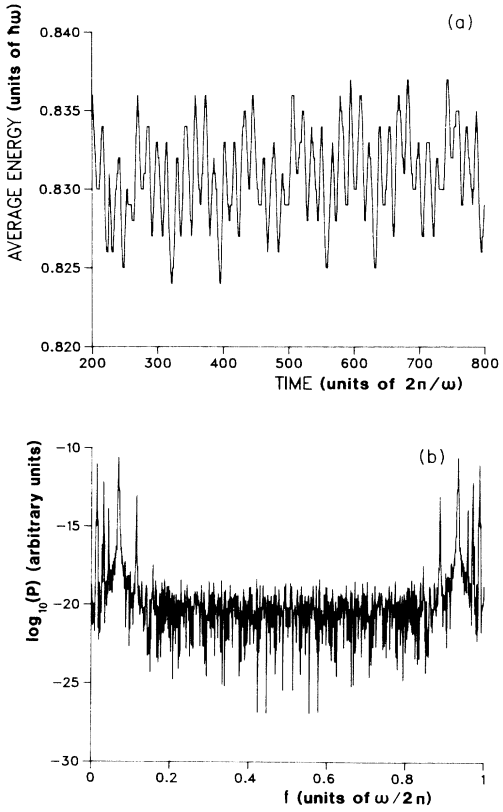

FIG. 10. (a) The time series of the oscillator energy $\langle E(t)\rangle$. The parameters ω_f, α, σ, and η are set at 4000 cm^{-1}, 0.86, 0.05, and 0.2. (b) The FFT power spectrum, $\log_{10}[P(f)]$, computed from the time series of (a).

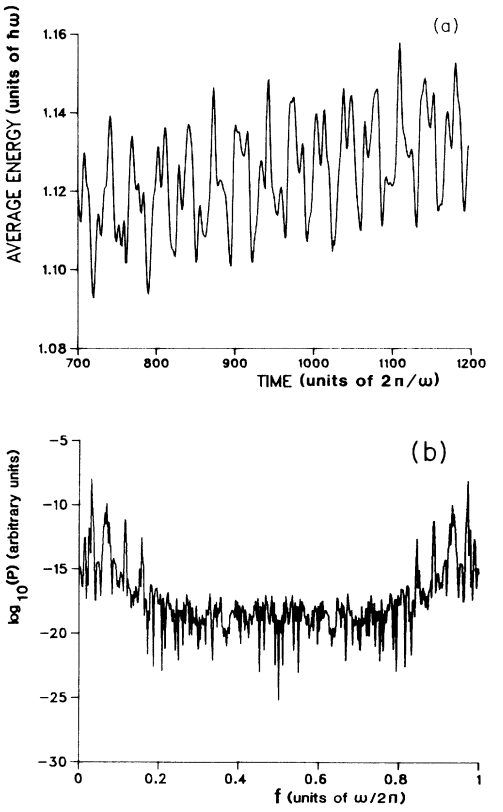

FIG. 11. (a) The time series of the oscillator energy $\langle E(t)\rangle$. The parameters ω_f, α, σ, and η are set at 4000 cm^{-1}, 1.57, 0.05, and 0.2. (b) The FFT power spectrum, $\log_{10}[P(f)]$, computed from the time series of (a).

Bimodal vibrational distributions have been seen in the experiments of infrared multiphoton excitation of SF_6 by Bagratashvili *et al.*[16,17] and Mazur, Burak, and Bloembergen.[18] In the former experiment the spectra of the Stokes signals from the Raman scattering have been determined. It was found that they have two well-separated peaks; one ensemble contains molecules which are vibrationally hot and the other vibrationally cold. This result is consistent with that observed by Mazur *et al.* in the anti-Stokes signal with low fluence.[18] Bagratashvili *et al.*[16,17] also showed that the effect of adding buffer Xe gas to SF_6 is to enhance the signal of the hot ensemble. The present model suggests one possible mechanism for the vibrational distribution to become bimodal. But since we are not simulating the multiphoton excitation process of SF_6 here, we cannot tell whether the present mechanism is indeed the one responsible for the bimodal distribution of SF_6. On the other hand, if we simulate the effects of the buffer gas by changing the phase relaxation rate η in our equations, then the results presented in Fig. 2 can be qualitatively interpreted as saying that the average oscillator energy increases with the pressure of the buffer gas, due to the fraction of the hot molecules increases, up to a pressure above which the excitation starts to go down. But again we should avoid the temptation of inferring too much from our results. Multiphoton excitation of SF_6 molecules is being investigated in our group by using the present model.

We note that in order to speed up the calculations the relaxation constants used in our study are much larger than the realistic values. Consequently, the laser intensity used here is also unpractically high. Even with the large damping constants used here the computation is still very time consuming. This prohibits, as mentioned above, the extensive study needed to unravel the bifurcation mechanism of the time series. For the latter investigations we may have to resort to approximate quantum methods. One of the methods[10] is to solve the Heisenberg equations for a truncated set of operators and then take the expectation values and introduce the factorization assumptions,[6] as was done in the semiclassical treatment.[5] The brute force solutions presented here can then serve as a benchmark for these approximate methods.

The dissociation continuum of an Morse oscillator is not included in an su(2) Hamiltonian. In order to consider the continuum we should use a noncompact group[23,24] such as an su(1,1) algebra.[23] This will, of course, be an important extension of the present treatment, for we can then investigate interesting processes

such as laser-induced dissociation of a molecule and desorption of surface-absorbed molecules. One goal that particularly concerns us here is to lower the threshold laser intensity for seeing interesting dynamic behavior. A possible answer to it is to choose weakly bound systems, but then the dissociation channel must be properly included. A weak link at the present time of the algebraic methods, either using su(2) or su(1,1), is that the expressions of the coordinate and momentum in terms of the generators of the group are still not known.

Another legitimate question to ask is whether hysteresis can be found at all in a quantum approach. In our opinion it is possible. For instance, a favorable situation is when the response of the bath is slow compared to the time scale of the molecular response[25,26] so that memory effects play a role. It is well known that delayed feedback often induces instabilities.[27,28] Other possibilities of seeing quantum hysteresis include formulations of dissipative quantum mechanics in which the equation of motion is nonlinear in the density matrix.[29] Until now our understanding of dissipative quantum mechanics[29,30] is rather limited and much more needs to be done along this direction.

ACKNOWLEDGMENTS

We are grateful to Dr. Helene Shapiro for the proof given in the Appendix. This work was supported by the Donors of the Petroleum Research Fund, administered by the American Chemical Society, and by the U. S. Army Research Office (Research Triangle Park, NC) under contract No. DAAG29-85-K-0256.

APPENDIX

We show in this appendix that any matrix A satisfying the following conditions has nonpositive real eigenvalues.

(1) A is a tridiagonal matrix.
(2) The column sums of A are zero.
(3) All diagonal elements are negative and off-diagonal elements positive.

The matrices associated with Eq. (2.18) and with ordinary master equations belong to this category.

A proof can be given in three steps.

Step 1. If T is a tridiagonal matrix, then we can find a diagonal matrix D such that $D^{-1}TD$ is symmetric and still tridiagonal.

Step 2. A real tridiagonal matrix must have real eigenvalues. This follows from step 1 and the fact that a real symmetric matrix has real eigenvalues.

Step 3. For the last step, we resort to a theorem due to Gerschgorin.[31,32] *Theorem:* Let A be an $n*n$ matrix. For each column i construct the circle centered at a_{ii} with radius equal to $\sum_{j\neq i} |a_{ji}|$. Then the eigenvalues of A lie in the union of these circles.

Since A has negative diagonal elements and positive off-diagonal ones, and the column sum of the off-diagonal ones equal to the absolute value of the diagonal element of that column, the Gerschgorin circles are all centered on the negative real axis and tangent to the imaginary axis at zero. Thus the eigenvalues lie in the left half plane. Since they are real, they must be zero or negative.

[1]G. C. Lie and J.-M. Yuan, J. Chem. Phys. **84**, 5486 (1986).
[2]J.-M. Yuan, in *Directions in Chaos*, edited by B. L. Hao (World Scientific, Singapore, in press).
[3]We have also found attractors which oscillate only on the attractive part of the potential curve. The oscillation coordinates of these attractors are 1 or 2 orders of magnitude larger than those of the attractors considered here. These attractors may correspond to dissociative states when thermal noise is inluded in the calculation.
[4]R. Kapral, M. Schell, and S. Fraser, J. Phys. Chem. **86**, 2205 (1982).
[5]J.-M. Yuan, E. Liu, and M. Tung, J. Chem. Phys. **79**, 5034 (1983).
[6]L. M. Narducci, S. S. Mitra, R. A. Shatas, and C. A. Coulter, Phys. Rev. A **16**, 247 (1977).
[7]A. O. Caldeira and A. J. Leggett, Ann. Phys. (N.Y.) **149**, 374 (1983).
[8]R. D. Levine, Chem. Phys. Lett. **95**, 87 (1983).
[9]R. D. Levine, in *Intramolecular Dynamics*, edited by J. Jortner and B. Pullman (Reidel, Dordrecht, 1982), p. 17.
[10]M. Tung, Ph.D dissertation, Drexel University, 1986.
[11]M. Tung, E. Eschenazi, and J.-M. Yuan, Chem. Phys. Lett. **115**, 405 (1985).
[12]We can replace A^+A^- of Eq. (2.6) by a linear combination of I_0 and A^+A^-.
[13]E. W. Montroll and K. E. Shuler, J. Chem. Phys. **26**, 454 (1957).
[14]W. H. Louisell and J. H. Marburger, IEEE J. Quantum Electron. **QE-3**, 348 (1967).
[15]R. Bonifacio and F. Haake, Z. Phys. **200**, 526 (1967).
[16]V. N. Bagratashvili, Y. G. Vainer, V. S. Dolzhikov, S. F. Kolyakov, V. S. Letokhov, A. A. Makarov, L. P. Malyarkin, E. A. Ryabov, E. G. Silkis, and V. D. Titov, Sov. Phys.—JETP **53**, 512 (1981).
[17]V. N. Bagratashvili, Y. G. Vainer, V. S. Doljikov, S. F. Kolyakov, V. S. Letokhov, A. A. Makarov, L. P. Malyarkin, E. A. Ryabov, and E. G. Silkis, Opt. Lett. **6**, 148 (1981).
[18]E. Mazur, I. Burak, and N. Bloembergen, Chem. Phys. Lett. **105**, 258 (1984).
[19]E. Liu and J.-M. Yuan, Phys. Rev. A **29**, 2257 (1984).
[20]A. Wolf, J. B. Swift, H. L. Swinney, and J. A. Vastano, Physica **16D**, 285 (1985). We have done calculations using a program listed in this paper.
[21]J. D. Farina, L. M. Narducci, J.-M. Yuan, and L. A. Lugiato, Opt. Eng. **19**, 469 (1980).
[22]See articles by M. Kus, K. Wodkiewicz, and J. A. C. Gallas, by H. J. Carmichael, C. M. Savage, and D. F. Walls, and by S. W. Koch, H. E. Schmidt, and H. Haug, in *Optical Bista-*

bility 2, edited by C. M. Bowden, H. M. Gibbs, and S. L. McCall (Plenum, New York, 1984).
[23]Y. Alhassid, J. Engel, and F. Iachello, Phys. Rev. Lett. **57**, 9 (1986).
[24]A. O. Barut, A. Inomata, and R. Wilson, J. Math. Phys. **28**, 605 (1987).
[25]B. Carmeli and D. Chandler, J. Chem. Phys. **82**, 3400 (1985).
[26]C. K. Chan and D. J. Kouri, J. Chem. Phys. **83**, 1750 (1985).
[27]K. Ikeda, H. Daido, and O. Akimoto, Phys. Rev. Lett. **45**, 709 (1980).
[28]J. Y. Gao, L. M. Narducci, H. Sadisky, M. Squicciarini, and J.-M. Yuan, Phys. Rev. A **30**, 901 (1984).
[29]H. J. Korsch and H. Steffen (unpublished).
[30]R. P. Parson and E. J. Heller, J. Chem. Phys. **85**, 2569 (1986).
[31]E. Bodewig, *Matrix Calculus* (North-Holland, Amsterdam, 1959), p. 67.
[32]F. M. Stein, *Introduction to Matrices and Determinants* (Wadsworth, Belmont, 1967), p. 149.